Article

Surface Structures of Rutile TiO (011)

Toshitaka Kubo, Hideo Orita, and Hisakazu Nozoye

J. Am. Chem. Soc., **2007**, 129 (34), 10474-10478• DOI: 10.1021/ja072281h • Publication Date (Web): 08 August 2007

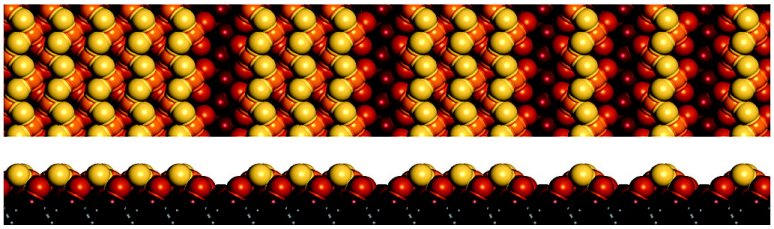

J|A|C|S
ARTICLES
Published on Web 08/08/2007

Surface Structures of Rutile TiO_2 (011)

Toshitaka Kubo,* Hideo Orita, and Hisakazu Nozoye†

Contribution from the National Institute of Advanced Industrial Science and Technology (AIST), Tsukuba Central 5-2, 1-1-1 Higashi, Tsukuba, Ibaraki 305-8565, Japan

Received April 2, 2007; E-mail: t-kubo@aist.go.jp

Abstract: Surface structures of rutile TiO_2 (011) are determined by a combination of noncontact atomic force microscopy (NC-AFM), scanning tunneling microscopy (STM), and density functional calculations. The surface exhibits rowlike ($n \times 1$) structures running along the [0$\bar{1}$1] direction. Microfaceting missing-row structural models can explain the experimental results very well. Calculated images for NC-AFM and STM are in good agreement with the experimental results. A decrease of the density of dangling bonds stabilizes the surface energy, which results in the microfaceting missing-row reconstructions.

1. Introduction

Considerable studies have been devoted to the surface of metal oxides,[1−31] because the surface of these materials has great technological importance, for example, for photocatalysis, sensors, solar cells, memory devises, and so on. In order to improve materials applications, numerous surface science techniques have been applied to gain a better understanding of the surface at an atomic level. It has become obvious that scanning tunneling microscopy (STM) has revolutionized the field of surface science; however, the interpretation of the images on metal oxide surfaces is often severely hampered by uncertainty as to whether the image contrast is governed by atomic- or electronic-structure effects.[4] As STM images are related to the shape of the wave functions near the Fermi level,[32] atoms which do not have the local density of states near the Fermi level are generally invisible even on the conductive materials. Noncontact atomic force microscopy (NC-AFM) is another scanning probe microscopy (SPM), whose imaging signal is not a tunneling current but an atomic force between a tip and a sample. NC-AFM has the possibility of providing a new aspect to the surface science of metal oxides because it has the potential to observe the atoms even on nonconductive materials. By combining the use of these two SPMs, surface atomic structures can be identified.[10−12,14,33]

Among metal oxide materials, rutile TiO_2 surfaces have been extensively studied as model systems to explore the surface physics and chemistry.[2−31] Although the physical property and chemical reactivity strongly depend on the surface orientation and its atomic structures, many of the structural works have been carried out mainly on the thermodynamically most stable (110) surface,[4−7,9,11−13,18,20,21,25−30] because the (110) surface is relatively easy to prepare among the rutile TiO_2 surfaces. Recently, more reactive surfaces have attracted considerable attention in relation to substrates for catalytic reac-

† Current address: ULVAC-PHI Inc., 370 Enzo, Chigasaki, Kanagawa, 253-0084, Japan.

(1) Henrich, V. E.; Cox, P. A. *The Surface Science of Metal Oxides*; Cambridge University Press: Cambridge, 1994.
(2) Murray, P. W.; Leibsle, F. M.; Muryn, C. A.; Fisher, H. J.; Flipse, C. F. J.; Thornton, G. *Phys. Rev. Lett.* **1994**, *72*, 689.
(3) Ramamoorthy, M.; Vanderbilt, D.; King-Smith, R. D. *Phys. Rev. B* **1994**, *49*, 16721.
(4) Diebold, U.; Anderson, J. F.; Ng, K. O.; Vanderbilt, D. *Phys. Rev. Lett.* **1996**, *77*, 1322.
(5) Guo, Q.; Cocks, I.; Williams, E. M. *Phys. Rev. Lett.* **1996**, *77*, 3851.
(6) Charlton, G.; Howes, P. B.; Nicklin, C. L.; Steadman, P.; Taylor, J. S. G.; Muryn, C. A.; Harte, S. P.; Mercer, J.; McGrath, R.; Norman, D.; Turner, T. S.; Thornton, G. *Phys. Rev. Lett.* **1997**, *78*, 495.
(7) Fukui, K. I.; Onishi, H.; Iwasawa, Y. *Phys. Rev. Lett.* **1997**, *79*, 4202.
(8) Lowekamp, J. B.; Rohrer, G. S.; Hotsenpiller, P. A. M.; Bolt, J. D.; Farneth, W. E. *J. Phys. Chem. B* **1998**, *102*, 7323.
(9) Bennett, R. A.; Stone, P.; Price, N. J.; Bowker, M. *Phys. Rev. Lett.* **1999**, *82*, 3831.
(10) Raza, H.; Pang, C. L.; Haycock, S. A.; Thornton, G. *Phys. Rev. Lett.* **1999**, *82*, 5265.
(11) Ashino, M.; Uchihashi, T.; Yokoyama, K.; Sugawara, Y.; Morita, S.; Ishikawa, M. *Phys. Rev. B* **2000**, *61*, 13955.
(12) Ashino, M.; Sugawara, Y.; Morita, S.; Ishikawa, M. *Phys. Rev. Lett.* **2001**, *86*, 4334.
(13) McCarty, K. F.; Bartelt, N. C. *Phys. Rev. Lett.* **1999**, *90*, 046104.
(14) King, D. A.; Woodruff, D. P. *The Chemical Physics of Solid Surfaces and Heterogeneous Catalysis, Vol. 9, Oxide Surfaces*; Elsevier: Amsterdam, 2001.
(15) Ohno, T.; Sarukawa, K.; Matsumura, M. *New J. Chem.* **2002**, *26*, 1167.
(16) Diebold, U. *Surf. Sci. Rep.* **2003**, *48*, 53.
(17) Wilson, J. N.; Idriss, H. *J. Catal.* **2003**, *214*, 46.
(18) Foster, A. S.; Pakarinen, O. H.; Airaksinen, J. M.; Gale, J. D.; Nieminen, R. M. *Phys. Rev. B* **2003**, *68*, 195410.
(19) Beck, T. J.; Klust, A.; Batzill, M.; Diebold, U.; Valentin, C. D.; Selloni, A. *Phys. Rev. Lett.* **2004**, *93*, 036104.
(20) Bredow, T.; Giordano, L.; Cinquini, F.; Pacchioni, G. *Phys. Rev. B* **2004**, *70*, 035419.
(21) Lindsay, R.; Wander, A.; Ernst, A.; Montanari, B.; Thornton, G.; Harrison, N. M. *Phys. Rev. Lett.* **2005**, *94*, 246102.
(22) Valentin, C. D.; Tilocca, A.; Selloni, A.; Beck, T. J.; Klust, A.; Batzill, M.; Diebold, U. *J. Am. Chem. Soc.* **2005**, *127*, 9895.
(23) Beck, T. J.; Klust, A.; Batzill, M.; Diebold, U.; Valentin, C. D.; Tilocca, A.; Selloni, A. *Surf. Sci.* **2005**, *591*, L267.
(24) Dulub, O.; Valentin, C. D.; Selloni, A.; Diebold, U. *Surf. Sci.* **2006**, *600*, 4407.
(25) Blanco-Rey, M.; Abad, J.; Rogero, C.; Mendez, J.; Lopez, M.F.; Martin-Gago, J.A.; de Andres, P. L. *Phys. Rev. Lett.* **2006**, *96*, 055502.
(26) Park, K. T.; Pan, M. H.; Meunier, V.; Plummer, E. W. *Phys. Rev. Lett.* **2006**, *96*, 226105.
(27) Lauritsen, J. V.; Foster, A. S.; Olesen, G. H.; Christensen, M. C.; Kühnle, A.; Helveg, S.; Rostrup-Nielsen, J. R.; Clausen, B. S.; Reichling, M.; Besenbacher, F. *Nanotechnology* **2006**, *17*, 3436.
(28) Pang, C. L.; Sasahara, A.; Onishi, H.; Chen, Q.; Thornton, G. *Phys. Rev. B* **2006**, *74*, 073411.
(29) Kiejna, A.; Pabisiak, T.; Gao, S. W. *J. Phys.: Condens. Matter* **2006**, *18*, 4207.
(30) Thompson, S. J.; Lewis, S. P. *Phys. Rev. B* **2006**, *73*, 073403.
(31) Kubo, T.; Sayama, K.; Nozoye, H. *J. Am. Chem. Soc.* **2006**, *128*, 4074.
(32) Tersoff, J.; Hamann, D. R. *Phys. Rev. B* **1985**, *31*, 805.
(33) Kubo, T.; Nozoye, H. *Phys. Rev. Lett.* **2001**, *86*, 1801.

10.1021/ja072281h CCC: $37.00

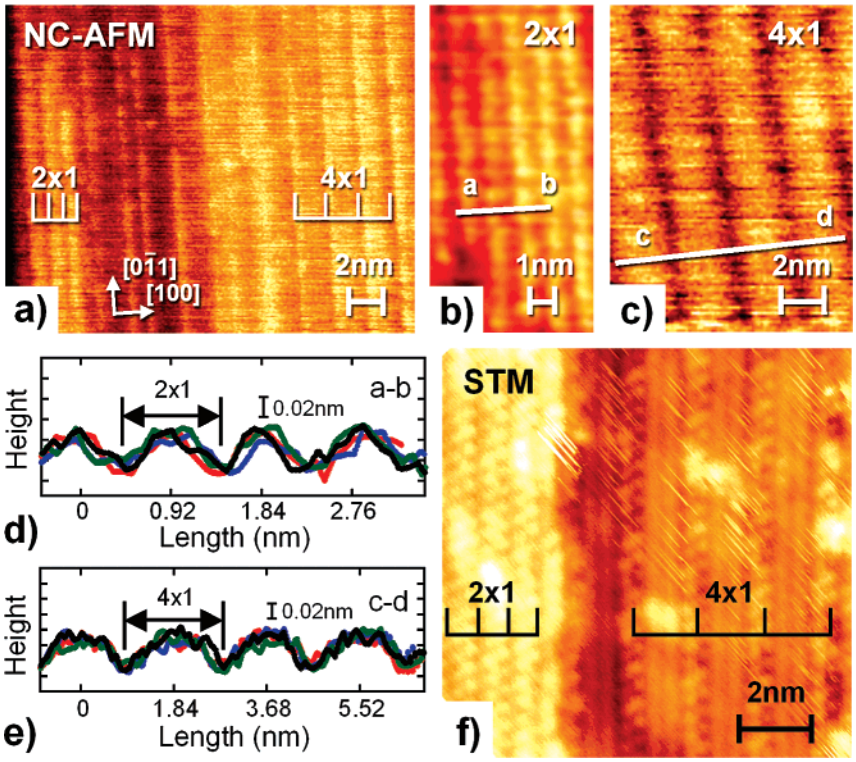

Figure 1. (a−c) NC-AFM and (f) STM ($V = +0.6$ V, $I = 0.02$ nA) images of TiO_2 (011) after heating at 800 °C. The image sizes are (a) 25 × 20 nm^2, (b) 6 × 12 nm^2, (c) 8 × 10.4 nm^2, and (f) 12 × 12 nm^2. Height profiles along the [100] direction of the (d) (2 × 1) and (e) (4 × 1) surface structures.

tions.[8,15,17,19,22−24,31] In particular, previous work suggests that the (011) surface showed a higher reactivity in catalytic reactions than other surfaces;[8,15,17] this surface of TiO_2 has a special importance. Here we present surface structural concepts, which are based on the combined utilization of NC-AFM, STM, and density functional calculations. The driving force of the reconstructions is discussed.

2. Experimental Section: Materials and Setup

Experiments were carried out in an ultrahigh vacuum scanning probe microscopy chamber (UHV-SPM) (JEOL model JAFM-4400) with a base pressure of $<1.4 \times 10^{-8}$ Pa. Cone-shaped silicon cantilevers with $f_0 = 150-320$ kHz and $k = 4.5-14$ N/m (Silicon-MDT Ltd.), which were highly doped with B (0.002 Ωcm) and coated with W_2C (25 nm thick, 30 μΩcm), were used for NC-AFM measurements. NC-AFM measurements were performed at room temperature under constant frequency shift conditions. Tips used for STM measurements were the same cantilevers as those used for NC-AFM or the tips made of a tungsten wire, 0.3 mm in diameter, by electrochemical etching in NaOH solution. STM measurements were performed at room temperature under constant current conditions.

A TiO_2 (011) substrate of 7 × 1 × 0.5 mm^3 (Nakazumi Crystal) was directly mounted on a silicon heater. The sample surface was cleaned by several cycles of Ar^+-ion sputtering (1 keV) and annealing. Vacuum pressure during annealing did not exceed 5×10^{-7} Pa. Temperature was measured with an optical pyrometer. As TiO_2 is a good insulator with a 3 eV band gap, STM can be applied only after the sample was heated. The conductivity arises from oxygen vacancy defect states near the Fermi level.

3. Theoretical Section: Calculation Details

The density functional theory (DFT) was employed in the implementation with plane waves, pseudo-potentials and generalized gradient approximation (GGA) along with the PW91 functional.[34] A plane wave cutoff of 300 eV and Monkhorst−Pack mesh of (4,4,2)−(1,4,1) were used. The criteria of energy change per atom, maximum displacement of atoms, and maximum force on each atom were 2.0×10^{-5} eV/atom, 0.002 Å, and 0.05 eV/Å, respectively. Gaussian smearing of 0.1 eV was used.

The crystal structure of rutile-type TiO_2 is tetragonal. The optimized bulk lattice parameters were $a = 4.665$ Å and $c = 2.961$ Å to be compared to the experimental values of $a = 4.584$ Å and $c = 2.953$ Å.[16] These lattice parameters were used for the slab calculations and were fixed throughout. The unreconstructed, the {111} microfaceting, and the titanyl (Ti═O) double-bond surfaces of TiO_2 (011) were modeled by periodic slabs. The periodic slabs were consisted of 4−10 atomic layers, which were isolated by 3 × $d_{TiO2(011)}$ width of vacuum regions. We used the slab models, whose two surfaces had the same atomic structure. All geometries were fully optimized without symmetry constraint and atom fixation.

4. Results and Discussion

Figure 1a shows an NC-AFM image of TiO_2 (011) after heating at 800 °C. The surface shows rowlike structures along the [0$\bar{1}$1] direction. Most of the structures are separated by dark rows with a distance of 0.92 or 1.84 nm, as shown in Figure 1b−e. These are, in good approximation, two or four times the lattice constant in the [100] direction ($a_{0[100]} = 0.46$ nm), respectively. From the distances between these rows, the surface is composed of (2 × 1) and (4 × 1) structures. In addition to these periodic structures, isolated missing (or added) rows can be seen. Figure 1f shows an STM image of a 12 × 12 nm^2 region of TiO_2 (011) after heating at 800 °C. The image is also composed of (2 × 1) and (4 × 1) structures. However, the STM image is quite different from the NC-AFM image. For the (2 × 1) region, the STM image shows bright rows, arranged in a zigzag pattern, along the [011] direction with the rows separated

(34) Segall, M. D.; Lindan, P. J. D.; Probert, M. J.; Pickard, C. J.; Hasnip, P. J.; Clark, S. J.; Payne, M. C. *J. Phys.: Condens. Matter* **2002**, *14*, 2717.

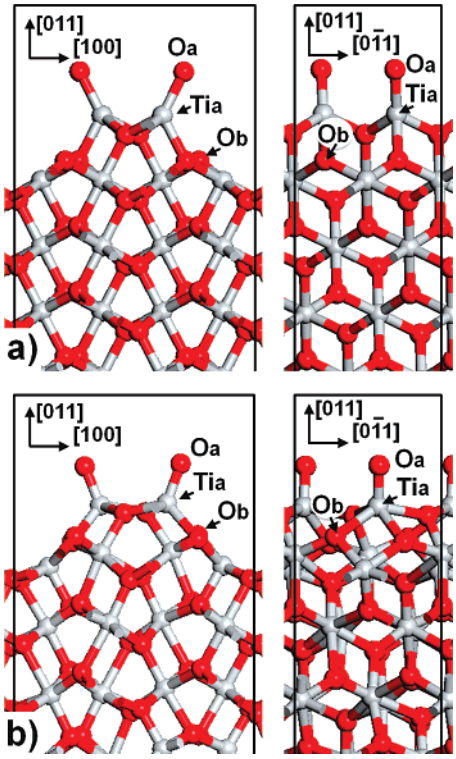

Figure 2. Structural models of (a) pre-optimized and (b) geometry-optimized titanyl (Ti═O) double-bond model, proposed by Beck et al.[19]

by 0.92 nm. For the (4 × 1) region, on the other hand, the STM image shows alternating dotlike bright rows and two linelike bright rows along the [0$\bar{1}$1] direction.

The present STM image of the (2 × 1) structure (Figure 1f) is the same as the results reported by Beck et al.[19] They proposed a structural model of the (2 × 1) reconstruction, i.e., titanyl (Ti═O) double-bond model, as shown in Figure 2. They concluded that the STM spots are related to the double-bonded O atoms (denoted by O_a) adsorbed on surface Ti atoms (denoted by Ti_a). In order to estimate the surface stability of their model, we discuss the surface energy (E_{surf}) and the atomic structure by calculations. The surface energy is calculated from the total energy of a super cell as follow: $2E_{surf} = E_{tot}(\text{supercell}) - nE_{tot}(\text{bulk})$. Here, $E_{tot}(\text{bulk})$ is the total energy of optimized bulk TiO_2 per TiO_2 unit, and $E_{tot}(\text{supercell})$ is the total energy of the given optimized super cell containing n TiO_2 units. The overall factor of 2 comes from the fact that each supercell had two surfaces with the same atomic structure. It should be noted that the physical properties, such as the surface energy, oscillate with the number of layers (odd−even oscillations).[3,20,29] When the thickness of the slab models is thin, the effect of the odd−even oscillations is more than several ten percent for the TiO_2 surface.[3,20,29] The surface energy also depends on the model symmetry and the existence of the fixed atoms.[3,29] Due to the electrostatic stabilizations for an ionic crystal, it is generally accepted that the accurate determination of surface energy requires the larger thickness of the slab,[3,20,29,30] higher slab symmetry,[3,20,29,30] and the slab to be fully optimized.[29] In the present study, we used the symmetric models whose two surfaces had the same atomic structure, and the error of the odd−even oscillations was less than the order of several percent. In our calculations, the calculated surface energy of the titanyl (Ti═O) double-bond model is about 30% larger (energetically less stable) than that of the bulk terminated TiO_2 (011)-(1 × 1) model. The results strongly suggest that the bulk terminated (011)-(1 × 1) surface does not reconstruct to form the titanyl (Ti═O) structure. Schematic illustrations of pre-optimized titanyl (Ti═O) double-bond model proposed by Beck et al. are shown in Figure 2a. The crystal structure of rutile-type TiO_2 is tetragonal and contains six atoms in a unit cell. Each Ti atom is coordinated to six neighboring O atoms, and each O atom is coordinated to three neighboring Ti atoms. As the Ti_a atoms of the titanyl fragments are fourfold coordinate in the pre-optimized titanyl (Ti═O) double-bond model, each Ti_a atom has two unsaturated dangling bonds (DBs). When this surface structural model is geometry optimized, the Ti_a atoms form an additional bond with the nearest-neighbor bridging O atoms (denoted by O_b), as shown in Figure 2b. These cause a large distortion in the surface and subsurface layers, which may lead the surface energy to be large (energetically less stable).

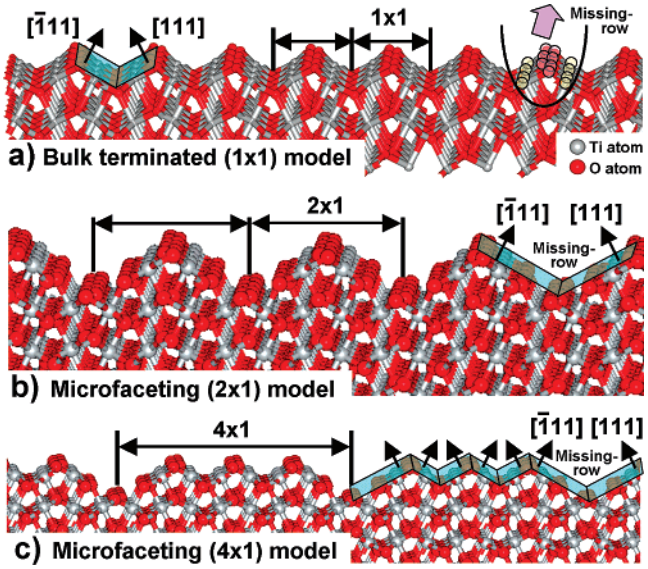

Figure 3. (a) Bulk terminated TiO_2(011)-(1 × 1) structural model. Proposed structural models of the microfaceting missing-row (b) (2 × 1) and (c) (4 × 1) surface reconstructions.

Although Beck et al. reported that the titanyl (Ti═O) double-bond model showed lower energy than that of the bulk terminated TiO_2 (011)-(1 × 1) model,[19] they used an asymmetric model; i.e., one surface is the titanyl (Ti═O) double-bond structure, and the other surface is the fixed bulk terminated TiO_2 (011)-(1 × 1). The asymmetry leads to a dipole moment along the surface normal direction, which affects the surface energy calculations considerably. The calculational error may be enhanced by using the asymmetric model[3,20,29,30] and the existence of the fixed layers.[3,29] For the titanyl (Ti═O) double-bond model, the double-bonded O_a atoms should be observed in the NC-AFM image. These suggest that the NC-AFM image of the (2 × 1) reconstruction should be almost the same as the STM image of the (2 × 1) reconstruction. However, the double-bonded O_a atoms are not observed, as shown in Figure 1b. The titanyl (Ti═O) double-bond model is not consistent with both the calculational results and the NC-AFM images of the (2 × 1) reconstruction.

Figure 3a shows a schematic illustration of the bulk terminated TiO_2 (011)-(1 × 1) surface. The surface has rows of fivefold coordinated Ti atoms and twofold coordinated O atoms (bridging oxygen atoms) along the bulk [0$\bar{1}$1] direction. The

rows are terminated by (111) and ($\bar{1}$11) microfacets. For the TiO_2 (011)-(2 × 1) surface, Diebold and co-workers reported that the surface is essentially stoichiometric by the use of UPS[19] and XPS.[24] For both the NC-AFM images of the (2 × 1) and (4 × 1) structures, the structures are separated by the dark rows running along the [0$\bar{1}$1] direction, as shown in Figure 1a−e. In order to explain both the results reported by Diebold and co-workers[19,24] and the present NC-AFM results, we propose microfaceting missing-row structural models in which rows of Ti_2O_2 units are removed on top of the surface, as shown in Figure 3b and c. At the missing row, the width of the {111} microfacets becomes wide and surface fivefold coordinated Ti atoms are replaced by the bridging O atoms. Supposing that the surface structures are based on the rutile-like geometry, there is no other acceptable model, which is consistent with all of the calculational and the experimental results.

NC-AFM images with highest lateral resolution originate with a short-range repulsive cantilever−sample interaction, such as Pauli repulsion,[33] chemical bonding,[35] and polar tip effect.[18,27,28] In the present study, because the chemical bonding features of the tip−sample interactions[35] were not detected, we concluded that the chemical bonding interaction was not dominant. Some experimental images and theoretical simulations of TiO_2 (110) show that the contrast over features happens to be completely reversed depending on the tip condition, when the polar materials accidentally terminate the AFM tip.[18,27,28] The polar materials (probably Ti^{4+} and O^{2-}) come from the surface of the sample. These may occur when reactive cantilevers are used.[27,28] On the other hand, we used less reactive W_2C coated cantilevers, and no change in imaging contrast was observed. In addition, when the polar materials terminate the tip apex, the local work function of the tip will change. However, these features were not observed either. These results suggest that the tips we used remained nonpolar. The less reactive- and the more stable- W_2C coated cantilever does not pick up the polar atoms from the sample surface. We concluded that the polar tip effect was excluded in our experimental conditions. Assuming that the tip−sample interaction is mainly due to the Pauli repulsion, which originates from the overlapping of the wave functions, we used the density functional calculations to analyze the occupied total charge density of states, as shown in Figure 4a and b. For both the (2 × 1) and (4 × 1) structures, the occupied total charge density of states is localized mainly at O atoms. The previous results reported by other laboratories also show that NC-AFM images on TiO_2 (110) directly trace the true surface topography.[10−12] In the present case, due to the broad shape of the occupied total charge density of states and the size of the apex of the NC-AFM cantilever, NC-AFM images are also broad. The calculated occupied total charge density of states explains the observed missing-row-like NC-AFM images well.

Next, in order to analyze the STM image, we discuss the shape of the orbital density near the Fermi level. Figure 4c and d show the equi-electron density surface, calculated by integrating the electronic states within an ∼1 eV window from the conduction band edge of the microfaceting missing-row models. The valence band of rutile TiO_2 is mainly O-2p derived while the empty conduction band is Ti-3d derived.[1,4,16] When a metal oxide sample is annealed in an ultrahigh vacuum, the sample is

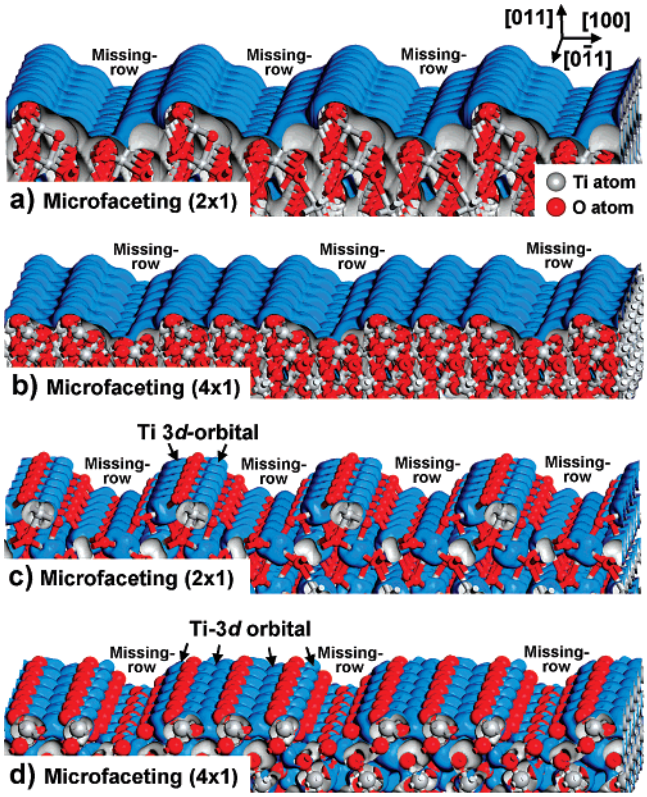

Figure 4. Calculated equi-electron density surface of the occupied total wave functions (blue surface represents the density level of 0.015 e/Å^3) of the microfaceting missing-row (a) (2 × 1) and (b) (4 × 1) structural models. Calculated equi-electron density surface near the Fermi level (blue surface represents the density level of 0.0015 e/Å^3) of the microfaceting missing-row (c) (2 × 1) and (d) (4 × 1) structural models, calculated by integrating the electronic states within an ∼1 eV window from the conduction band edge.

generally reduced; i.e., oxygen vacancy defects are formed. As one oxygen vacant site can provide two electrons, which occupy the Ti-3d states near the conduction band bottom, oxygen vacancy states pin the Fermi level at (or close to) the conduction band edge. It is generally accepted that the observed STM spots on rutile TiO_2 surfaces are mainly related to the surface Ti atoms.[2,4,10] In the present case, the calculated results also show that all the wave functions near the bottom of the conduction bands are localized at the Ti atoms, as shown in Figure 4c and d. Figure 5 shows schematic illustrations of the Ti-3d orbitals of the surface Ti atoms. For the (2 × 1) structure, STM spots, arranged in a zigzag pattern, correspond to the surface fivefold Ti atoms at the missing row. For the (4 × 1) structure, STM spots of the dotlike bright rows and linelike bright rows correspond to the surface fivefold Ti atoms at the missing row and bulk terminated (1 × 1) row, respectively. The conclusion that surface fivefold Ti atoms are imaged is in agreement with STM observation. In addition, as the Ti-3d orbitals of the surface fivefold Ti atoms act as preferential adsorption sites for atoms and molecules, the adsorption behaviors of the light molecules, such as water and formic acid, are quite reasonable in our structural model.[19,22,23] Recently, Dulub et al. observed O-deficient type defects at the vacuum-annealed surface of bulk-reduced TiO_2 (011)-(2 × 1) samples by STM.[24] They concluded that the defects were related to the O vacancies of the titanyl fragments. However, the microfaceting missing-row model can also explain their results well. In the case of the microfaceting

(35) Uchihashi, T.; Sugawara, Y.; Tsukamoto, T.; Ohta, M.; Morita, S. *Phys. Rev. B* **1997**, *56*, 9834.

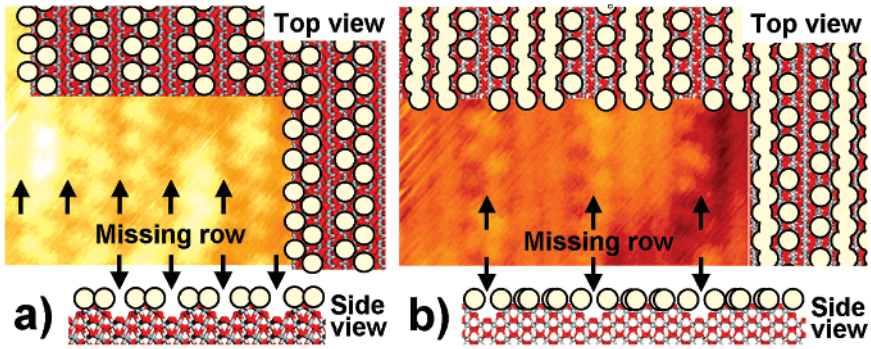

Figure 5. Schematic illustration of the STM images of the microfaceting missing-row (a) (2 × 1) and (b) (4 × 1) structural models. A circle shows the position of the surface Ti-3d orbitals.

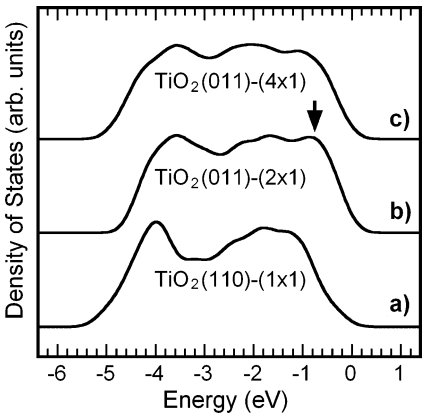

Figure 6. Calculated density of states of (a) TiO_2(110)-(1 × 1), TiO_2-(011) microfaceting missing-row (b) (2 × 1) and (c) (4 × 1) models. The energy zero is at the upper edge of the valence band.

missing-row model, a single Ti atom cannot be removed from the top surface, due to the surface energetic stability. The defects should be the TiO_4 vacancies on the top surface rows, and observed STM darker spots[24] are considered to be the Ti-3d orbitals of the next layer of Ti atoms. When the samples are reduced, the O-deficient type TiO_4 vacancy defects are formed. The structural concept of the microfaceting missing row is quite reasonable, compared with the experimental results reported previously.[19,22−24]

The calculated electronic density of states for the TiO_2 (110)-(1 × 1), TiO_2 (011) microfaceting missing-row (2 × 1) and (4 × 1) models are shown in Figure 6. For the TiO_2 (011)-(2 × 1) surface, Beck et al. observed a small photoemission peak at the upper edge of the valence band.[19] The corresponding peak was not observed on TiO_2 (110)-(1 × 1). They concluded that the small peak originates from the O titanyl atoms of their titanyl (Ti═O) double-bond model. As shown in Figure 6b, a well-defined peak is also present for the TiO_2 (011) microfaceting missing-row (2 × 1) models (denoted by arrow). These calculational results suggest that our structural model can explain their experimental results well.

Finally, we mention the driving force of the microfaceting missing-row reconstructions. Atoms on a surface are generally less stable compared with those at a bulk position, because of the absence of neighboring atoms on one side. In order to reduce surface energy, many surfaces exhibit various reconstructions. In the case of semiconductor surfaces, the surface energy mainly comes from the unsaturated dangling bonds that are left on the surface.[36,37] Then there is certainly a tendency of decreasing free dangling bonds on many reconstructed surfaces. In the present case, decreasing the density of dangling bonds of Ti atoms (n_{DBs}) may contribute to the surface energy and result in the reconstructions. To discuss the relative surface energies per Ti dangling bond, the density of Ti dangling bonds and calculated surface energies of the various orientations are summarized in Table 1. Different crystal planes have different numbers of atoms per unit area, and they will have different numbers of dangling bonds per unit area and exhibit different surface energies. However, calculated surface energies per Ti dangling bond (E_{surf}/n_{DBs}) are almost the same (∼0.8 eV). The results suggest that the surface energy of rutile TiO_2 is also related to the density of Ti dangling bonds. The formation of the missing row decreases the density of Ti dangling bonds. When compared with the bulk terminated TiO_2 (011)-(1 × 1) structure, the density of Ti dangling bonds of the TiO_2 (011)-(2 × 1) and (4 × 1) microfaceting missing-row structures are $^1/_2$ and $^3/_4$, respectively. The decrease of the density of dangling bonds is considered to be one of the driving forces of the surface reconstructions on rutile TiO_2 (011).

Table 1. Density of Ti Dangling Bonds (n_{DBs}) and Calculated Surface Energy (E_{surf}) for Several 1 × 1 Surfaces of Different Orientations[a]

surface	n_{DBs}	E_{surf}	E_{surf}/n_{DBs}
(110)	1.46×10^{-2}	12.1	0.83
(011)	2.24×10^{-2}	17.5	0.78
(001)	2.67×10^{-2}	23.4	0.88

[a] The n_{DBs}, E_{surf}, and E_{surf}/n_{DBs} values are in units of au^{-2}, meV/au^2, and eV, respectively.

5. Conclusion

In conclusion, we have used NC-AFM, STM, and density functional calculations to elucidate the nature of the surface reconstructions of rutile TiO_2 (011). The microfaceting structural models, whose structural concept is the same as that we have recently reported on for the rutile TiO_2 (001) surface,[31] can also explain both the experimental results and the theoretical calculations of the surface reconstructions of rutile TiO_2 (011). A decrease of the density of dangling bonds stabilizes the surface energy, which results in the microfaceting missing-row reconstructions.

JA072281H

(36) King, D. A.; Woodruff, D. P. *The Chemical Physics of Solid Surfaces and Heterogeneous Catalysis, Vol. 5, Surface Properties of Electronic Materials*; Elsevier: Amsterdam, 1988.
(37) Lüth, H. *Surfaces and Interfaces of Solid Materials*; Springer: New York, 1995.